Assessment of the performance of various airfoil sections on power generation from a wind turbine using the blade element momentum theory

Xiaomin Chen, Ramesh Agarwal

Department of Mechanical Engineering & Materials Science, Washington University in St. Louis, Jolley Hall, Campus Box 1185, One Brookings Drive, St. Louis, Missouri, 63130, USA.

Abstract
It is well established that the power generated by a Horizontal-Axis Wind Turbine (HAWT) is a function of the number of blades B, the tip speed ratio λ (blade tip speed/wind free stream velocity) and the lift to drag ratio (C_L / C_D) of the airfoil sections of the blade. The airfoil sections used in HAWT are generally thick airfoils such as the S, DU, FX, Flat-back and NACA 6-series of airfoils. These airfoils vary in (C_L / C_D) for a given B and λ, and therefore the power generated by HAWT for different blade airfoil sections will vary. The goal of this paper is to evaluate the effect of different airfoil sections on HAWT performance using the Blade Element Momentum (BEM) theory. In this study, we employ DU 91-W2-250, FX 66-S196-V1, NACA 64421, and Flat-back series of airfoils (FB-3500-0050, FB-3500-0875, and FB-3500-1750) and compare their performance with S809 airfoil used in NREL Phase II and III wind turbines; the lift and drag coefficient data for these airfoils sections are available. The output power of the turbine is calculated using these airfoil section blades for a given B and λ and is compared with the original NREL Phase II and Phase III turbines using S809 airfoil section. It is shown that by a suitable choice of airfoil section of HAWT blade, the power generated by the turbine can be significantly increased. Parametric studies are also conducted by varying the turbine diameter.
Copyright © 2013 International Energy and Environment Foundation - All rights reserved.

Keywords: Wind energy; Wind turbine blade airfoils; Blade element momentum theory.

1. Introduction
Because of recent emphasis on carbon free renewable energy, there has been great deal of research directed towards the design of aerodynamically efficient wind turbines. There are mainly two kinds of wind turbines: Horizontal –Axis Wind Turbines (HAWT) and Vertical-Axis Wind Turbines (VAWT). Between them, HAWTs are the most commercially deployed turbines all over the world since they are able to generate more electricity at a given wind speed, especially in large wind farm applications when the wind is intermittent [1]. This study focuses on improving the HAWT performance by changing the blade airfoil sections while the chord length and the twist angle along the blade span are kept fixed.
In order to calculate the wind turbine power, a Java-based aerodynamic analysis tool using Blade Element Momentum Theory has been developed based on Ceyhan's method [2]. The BEM analysis tool is validated against the field test data and Ceyhan's BEM results for two wind turbines: NREL (National Renewable Energy Laboratory, USA) Phase II and III wind turbines. The NREL Phase II wind turbine has an untwisted and un-tapered blade while the NREL Phase III wind turbine has a twisted and un-

tapered blade. Validations are performed to show the capabilities of our BEM analysis tool. The developed BEM tool is accurate and efficient in calculating the wind turbine performance based on comparisons with the test data.

The airfoil sections used in this study are thick airfoils. They were used as the baseline airfoils for shape optimization using genetic algorithms in previous studies [3, 4] by the authors because of their aerodynamic and structural advantages [5]. In this study we employ FB series (FB-3500-0050, FB-3500-0875, FB-3500-1750) [6], FX 66-S196-V1 [7], DU 91-W2-250 [8] and NACA 64421 [9] airfoils. Their aerodynamic characteristics including C_L and C_D are collected and expanded to a wider range of angles of attack for BEM calculation. The wind power calculation results for blades with these airfoil sections are compared with the NREL Phase II wind turbine. It is shown that thick airfoil sections can increase the wind turbine power by as much as 100 percent.

2. Brief overview of the blade element momentum (BEM) theory

This study employs Blade Element Momentum Theory for calculation of power output of a HAWT. The BEM theory models the axial and tangential induction factors by equating the force and torque relations for a small ring in the turbine plane (modeled as an actuator disk) derived from either the momentum theory or the blade element theory [2].

2.1 Momentum theory

In the momentum theory, we consider the stream tube surrounding the wind turbine which is modeled as an actuator disc as shown in Figure 1. Assuming steady, uniform, axisymmetric, incompressible, inviscid flow with a nonrotating wake, the mass conservation in the stream tube gives the following relation:

$$\rho U_1 A_1 = \rho U_2 A_d = \rho U_4 A_4 \qquad (1)$$
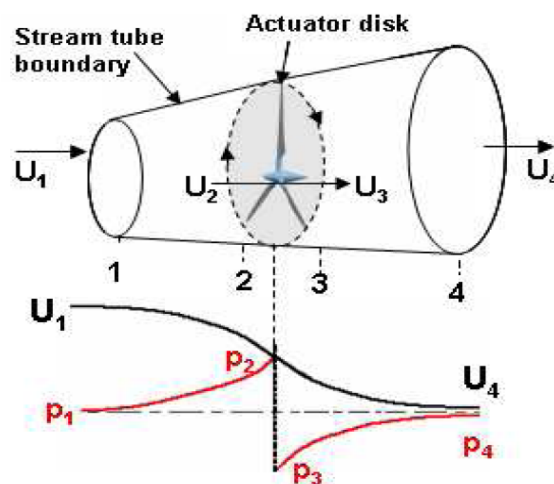
where A_d is area of the actuator disk.

Figure 1. Actuator disk model of a wind turbine [2]

Since the actuator disc induces velocity in the stream tube, an axial induction factor a is defined as:

$$a = \frac{U_1 - U_2}{U_1} \qquad (2)$$

Thus, we have

$$U_2 = U_1(1 - a) \qquad (3)$$

$$U_4 = U_1(1 - 2a) \tag{4}$$

Applying the Bernoulli equations to point 1, 2 and 3, 4, we can derive the following expression for pressure difference across the actuator disk:

$$p_2 - p_3 = \frac{1}{2}\rho(U_1^2 - U_4^2) \tag{5}$$

Thus, the net force normal to the plane on a ring of width dr in the actuator disk can be calculated as:

$$dN = (p_2 - p_3)dA_d = 4\rho U_1^2 a(1-a)\pi r\,dr \tag{6}$$

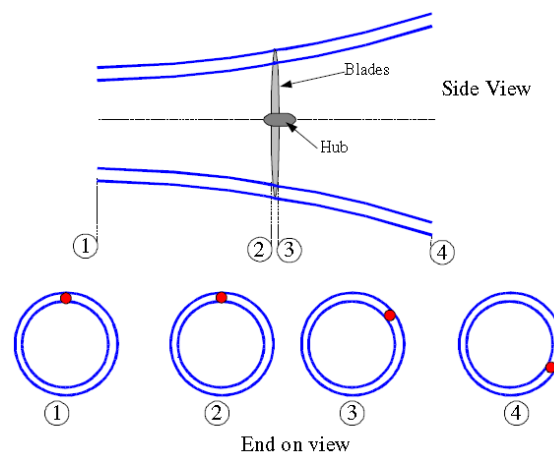Now, we consider the rotating annular stream tube shown in Figure 2.

Figure 2. Rotating annular stream tube [10]

Define an angular induction factor a' as:

$$a' = \frac{\omega}{2\Omega} \tag{7}$$

where ω is the angular velocity of the blade wake and Ω is the angular velocity of the blade. For a small element dr, the corresponding torque is given by:

$$dQ = \rho 2\pi r\,dr\,U_2\omega r^2 \tag{8}$$

Together with (7), the torque is calculated as:

$$dQ = 4a'(1-a)\rho U_1\Omega r^3\pi\,dr \tag{9}$$

2.2 Blade element theory
In the blade element theory, the blade is assumed to be divided into N sections which are called the blade elements. It is assumed that there is zero aerodynamic interaction between the blade elements and there is negligible spanwise velocity component on the blade. The forces on the blade element are solely determined by the lift and drag characteristics of 2D airfoils of the blade element; lift and drag components are defined perpendicular and parallel to the relative wind speed direction. The total tangential velocity experienced by the blade element is $(1+a')\Omega r$ and the axial velocity is $(1-a)U_\infty$. The relative wind velocity at the blade is given by:

$$W = \frac{U_\infty (1-a)}{\sin \phi} \tag{10}$$

The angle between the relative wind velocity and the plane of rotation is given by:

$$\tan \phi = \frac{U_\infty (1-a)}{\Omega r (1-a')} = \frac{(1-a)}{(1-a')\lambda_r} \tag{11}$$

where λ_r is the local tip speed ratio.

The net force normal to the plane of rotation for each blade element and the resulting torque on each blade element can be written as:

$$dN = dL \cos \phi + dD \sin \phi \tag{12}$$

$$dQ = r(dL \sin \phi - dD \cos \phi) \tag{13}$$

where dL and dD are the lift and drag forces on the blade elements respectively. They are defined as:

$$dL = C_L \frac{1}{2} \rho W^2 c dr \tag{14}$$

$$dD = C_D \frac{1}{2} \rho W^2 c dr \tag{15}$$

For a multi-bladed wind turbine with B number of blades, one can write:

$$dN = B \frac{1}{2} \rho W^2 (C_L \cos \phi + C_D \sin \phi) c dr \tag{16}$$

$$dQ = B \frac{1}{2} \rho W^2 (C_L \sin \phi - C_D \cos \phi) c r dr \tag{17}$$

Defining the local solidity as $\sigma' = \frac{Bc}{2\pi r}$ and replacing W with equation (10), equations (16) and (17) become:

$$dN = \sigma' \pi \rho \frac{U_\infty^2 (1-a)^2}{\sin^2 \phi} (C_L \cos \phi + C_D \sin \phi) r dr \tag{18}$$

$$dQ = \sigma' \pi \rho \frac{U_\infty^2 (1-a)^2}{\sin^2 \phi} (C_L \sin \phi - C_D \cos \phi) r^2 dr \tag{19}$$

2.3 Tip loss correction and modified BEM theory
The original BEM theory does not include 3D characteristics of the flow and viscous losses due to separation and turbulence. Some modification needs to be applied to the theory to take into account these losses. The modified BEM theory includes the tip-loss and Glauert corrections [11]. The tip-loss model serves to correct the induced velocity resulting from the vortices shed from the blade tips into the wake on the induced velocity field while the hub-loss model corrects the induced velocity resulting from a vortex being shed near the hub of the rotor [11]. These losses are calculated as:

$$F_{tip} = \frac{2}{\pi}\cos^{-1}\left(\exp\left(-\frac{B}{2}\frac{R-r}{r\sin\phi}\right)\right) \tag{20}$$

$$F_{hub} = \frac{2}{\pi}\cos^{-1}\left(\exp\left(-\frac{B}{2}\frac{r-r_{hub}}{r_{hub}\sin\phi}\right)\right) \tag{21}$$

The net tip loss is given by

$$F = F_{tip} * F_{hub} \tag{22}$$

The Glauert empirical relation with a modification for the tip loss factor is given as:

$$C_T = \frac{8}{9} + (4F - \frac{40}{9})a + (\frac{50}{9} - 4F)a^2 \tag{23a}$$

$$a = \frac{18F - 20 - 3\sqrt{C_T(50-36F)+12F(3F-4)}}{36F-50} \tag{23b}$$

After considering tip loss and Glauert correction, we have four equations - (24) and (25) derived from the momentum theory and (26) and (27) obtained from blade element theory:

$$dN = 4F\rho U_1^2 a(1-a)\pi r \, dr \tag{24}$$

$$dQ = 4Fa'(1-a)\rho U_1 \Omega r^3 \pi \, dr \tag{25}$$

$$dN = \sigma'\pi\rho\frac{U_\infty^2(1-a)^2}{\sin^2\phi}(C_L\cos\phi + C_D\sin\phi)r dr \tag{26}$$

$$dQ = \sigma'\pi\rho\frac{U_\infty^2(1-a)^2}{\sin^2\phi}(C_L\sin\phi - C_D\cos\phi)r^2 dr \tag{27}$$

By equating the force relation (24) and (26) and torque relation (25) and (27), the axial induction factor a and the angular induction factor a' can be calculated. The process to calculate the induction factors is an iterative process shown in Figure 3. When the iteration converges, the induction factors can be determined and are then used to calculate the angles of attacks and thrust for each blade element separately for the wind turbine performance analysis. The total power from the rotor is given by:

$$P = \int_{rh}^{R} dP = \int_{rh}^{R} \Omega dQ \tag{28}$$

3. Airfoil data preparation
As shown in the BEM iteration process in Figure 3 for induction factors calculation, aerodynamic characteristics (C_L and C_D) of airfoils are needed to determine the thrust coefficient C_T. This study employs the airfoils shapes including S809 [12], FB series (FB-3500-0050, FB-3500-0875, FB-3500-1750), FX 66-S196-V1, DU 91-W2-250 and NACA 64421 airfoils. Their experimental data are available in the open literature for a range of angles-of-attack (usually from -5 to 15 degrees) and Reynolds numbers [6, 9, 13]. However, in the actual operation of a wind turbine, the blades experience very high angle-of-attack regimes. The currently available data needs to be expanded to cover high angles-of-attack regimes. This study uses Viterna's method in AirfoilPrep v2.2 developed by NREL [14] as the

extrapolation tool to construct the C_L and C_D data between -180 and +180 degrees of angles of attack. The Reynolds numbers are chosen as some appropriate fixed numbers. Figure 4 shows an example of airfoil data extrapolation for DU 91-W2-250 airfoil.
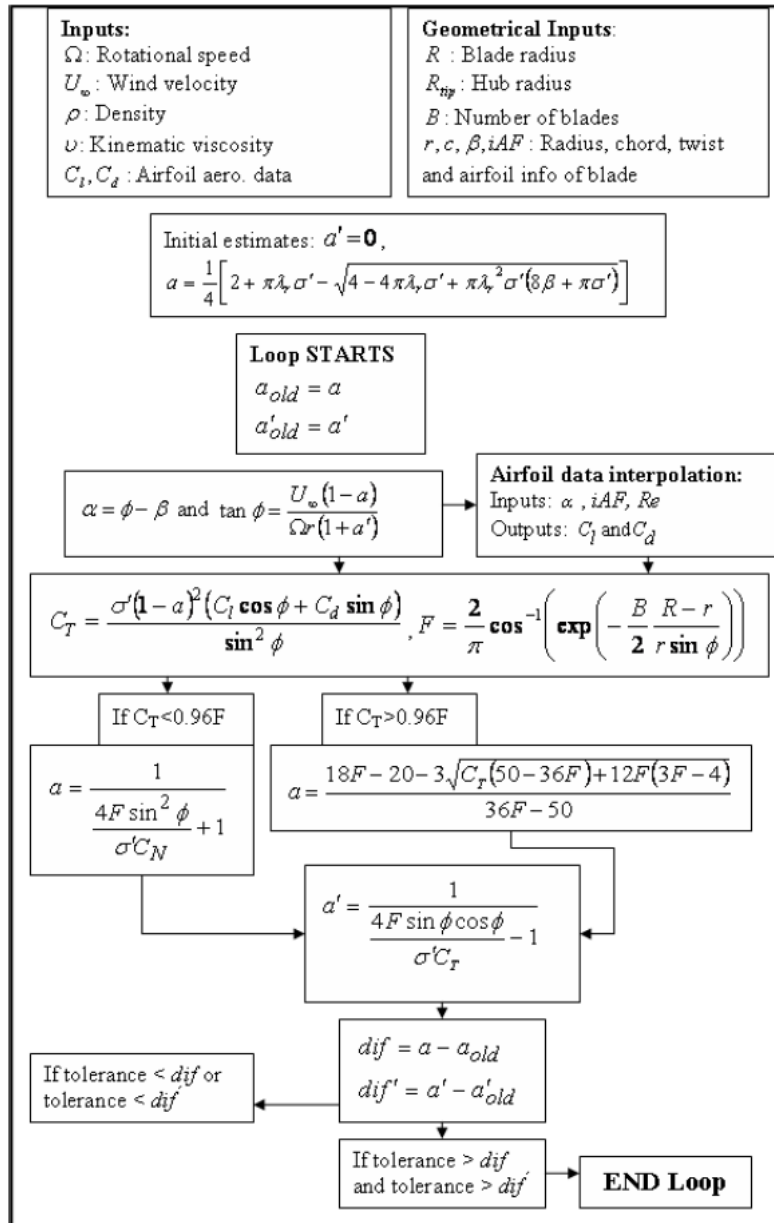

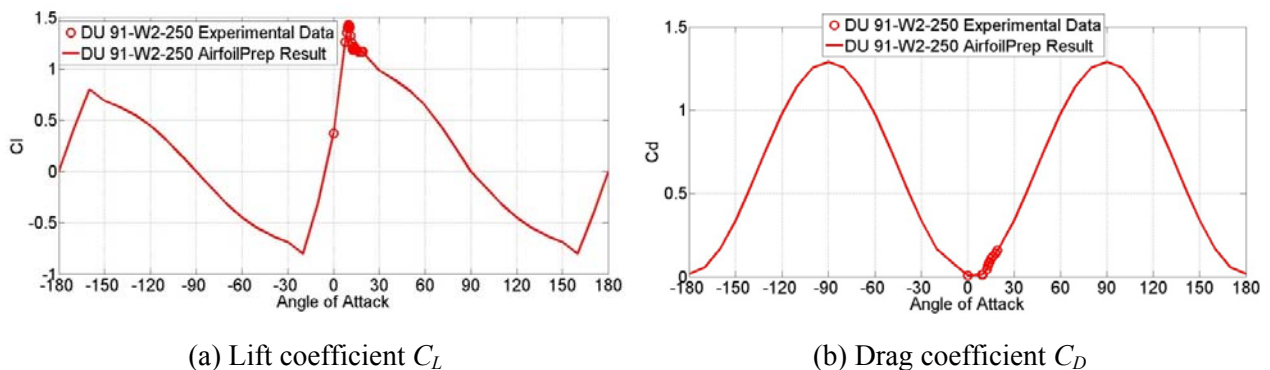Figure 3. Iterative procedure for induction factors calculation

(a) Lift coefficient C_L (b) Drag coefficient C_D

Figure 4. Airfoil data extrapolation compared with the original experimental data

4. Results and discussion

4.1 Validation of BEM analysis tool

Before calculating the wind turbine power using thick airfoils, BEM code validations are performed to assess its accuracy and efficiency. Three different wind turbines are employed in the validation process. The calculated results are compared with the experimental data in Reference [12] and the BEM results of Ceyhan [2]. The first validation case is for the NREL untwisted and un-tapered blade wind turbine known as the NREL Phase II wind turbine. The wind turbine employs S809 airfoil section along the blade without any twist and taper. The operating conditions and geometrical properties are shown in Table 1 and Figure 5. The second validation case is the NREL twisted and un-tapered wind turbine called NREL Phase III wind turbine. It adds some twist to the turbine blade along the blade span. Table 2 and Figure 6 show the operating conditions and geometrical properties. The third validation case is the Risoe wind turbine. This wind turbine has both twist and taper in the blades. In Risoe wind turbine, NACA 63-2xx series airfoils are used. Table 3 and Figure 7 show the operating conditions and geometrical properties of Risoe wind turbine.

Table 1. NREL Phase II wind turbine general characteristics

Number of Blades	3
Turbine Diameter	10.06 m
Rotational Speed	71.3 rpm
Cut-in Wind Speed	6 m/s
Control	Stall Control
Rated Power	19.8 kW
Root Extension	0.723 m
Blade Set Angle	12 degrees
Twist	None
Chord	0.4572@all span location
Airfoil	S809

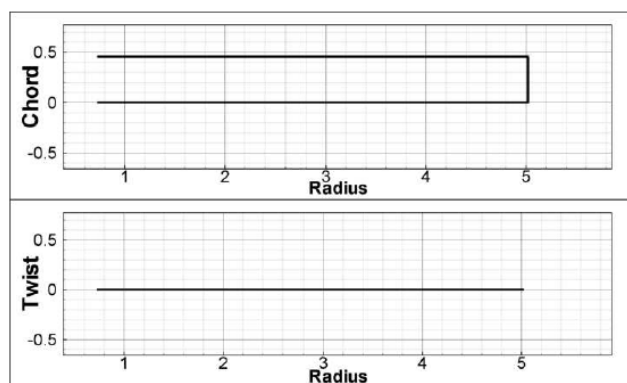Figure 5. Geometric properties of NREL Phase II wind turbine

Table 2. NREL Phase III wind turbine general characteristics

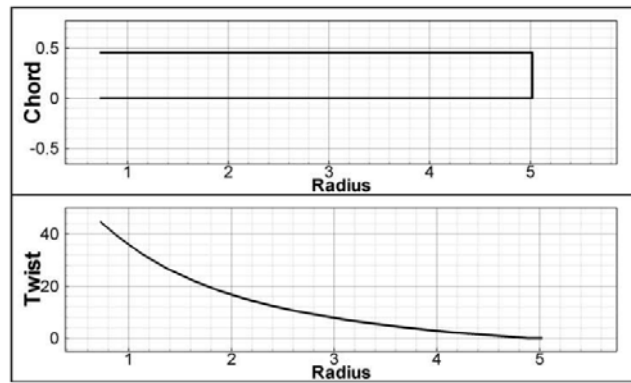|	
Number of Blades	3
Turbine Diameter	10.06 m
Rotational Speed	71.3 rpm`
Cut-in Wind Speed	6 m/s
Control	Stall Control
Rated Power	19.8 kW
Root Extension	0.723 m
Blade Set Angle	3 degrees
Twist	44 degrees (max.)
Chord	0.4572@all span location
Airfoil	S809

Figure 6. Geometric properties of NREL Phase III wind turbine

Table 3. Risoe wind turbine general characteristics

Number of Blades	3
Turbine Diameter	19.0 m
Rotational Speed	35.6 and 47.5 rpm`
Cut-in Wind Speed	4 m/s
Control	Stall Control
Rated Power	100 kW
Root Extension	2.3 m
Blade Set Angle	1.8 degrees
Twist	15 degrees (max.)
Root Chord	1.09 m
Tip Chord	0.45 m
Airfoil	NACA 63-2xx series
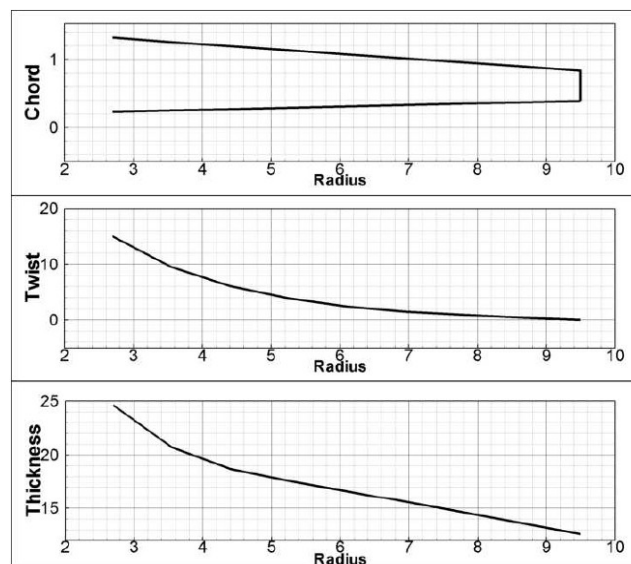
Figure 7. Geometric properties of Risoe wind turbine

Figures 8, 9 and 10 show the comparison of results among NREL Phase II, NREL Phase III and Risoe wind turbines. These three figures show that the BEM analysis tool employed in this study performs quite well in matching the experimental data for a wide range of wind speeds, especially at high wind speeds (greater than 8 m/s). The improvement in comparisons between the test data and computations at small wind speeds (lower than 8 m/s) requires more accurate C_L and C_D data. Considering that most large scale wind turbines operate at high wind speed, the validation results are acceptable and the BEM analysis tool can be considered as a good code to estimate the power output from a wind turbine using thick airfoils mentioned before.
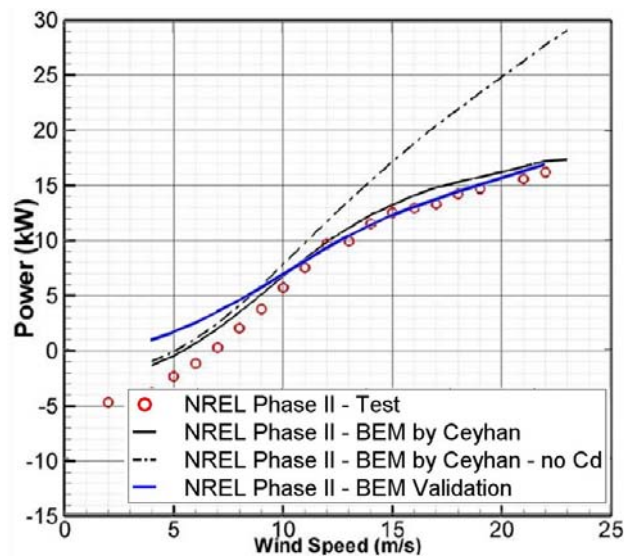
Figure 8. Comparison of BEM calculations with test data for NREL Phase II wind turbine
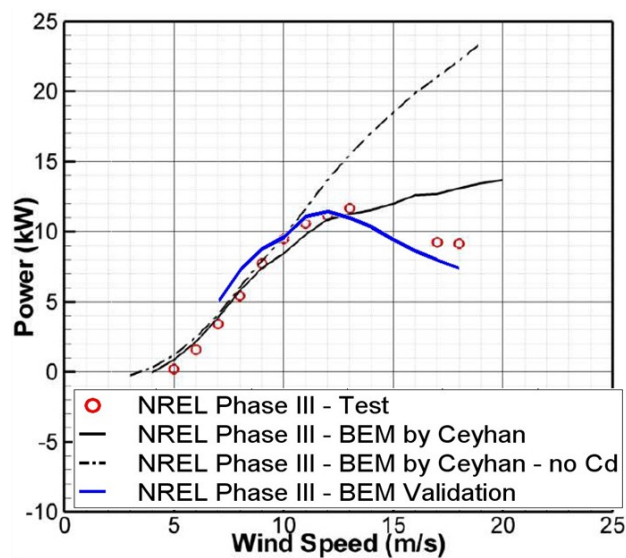

Figure 9. Comparison of BEM calculations with test data for NREL Phase III wind turbine
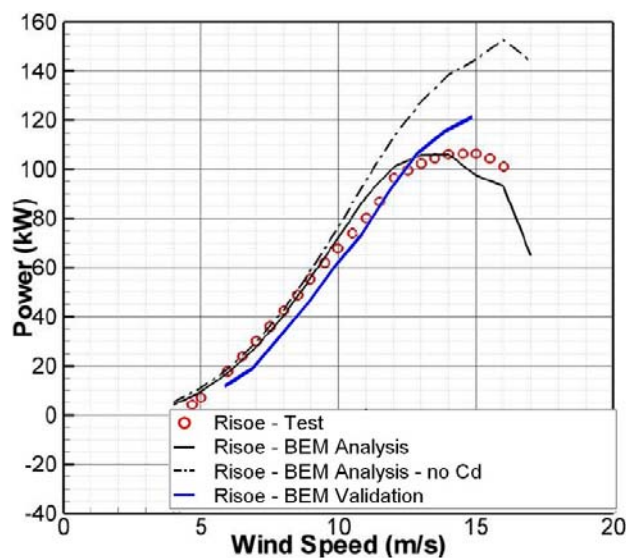

Figure 10. Comparison of BEM calculations with test data for Risoe wind turbine

4.2 Results and discussion for turbines with thick airfoils

In this section, we analyze the performance of various wind turbines (NREL Phase II and Phase III, and Risoe) using thick airfoil sections for their blades employing our BEM code. The power output of turbines is computed with new airfoil sections for blades and is compared with original NREL Phase II and Phase III, and Risoe turbines. Table 4 and Figure 11 show the operating conditions and geometrical properties of the wind turbines with untwisted and un-tapered blades using a variety of thick airfoil sections. Figure 12 shows the power output of the wind turbines using different airfoil sections in Table 4 and their comparison with the original NREL Phase II wind turbine with S809 airfoil section for its blades.

Table 4. General characteristics of wind turbine using thick airfoil sections

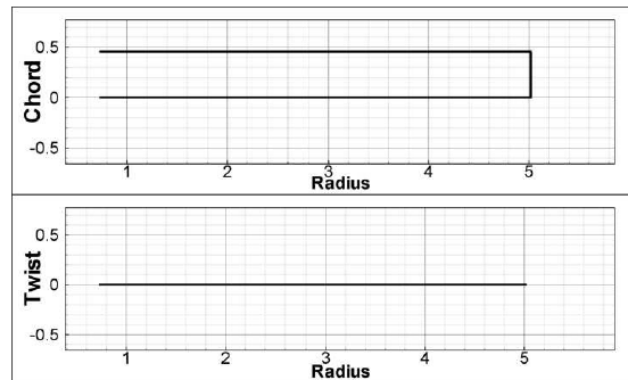|	
Number of Blades	3
Turbine Diameter	10.06m
Rotational Speed	71.3rpm`
Cut-in Wind Speed	6 m/s
Control	Stall Control
Rated Power	19.8kw
Root Extension	0.723m
Blade Set Angle	12 degrees
Twist	None
Chord	0.4572@all span location
Airfoil Sections	FB series (FB-3500-0050, FB-3500-0875, FB-3500-1750), FX 66-S196-V1, DU 91-W2-250, NACA 64421

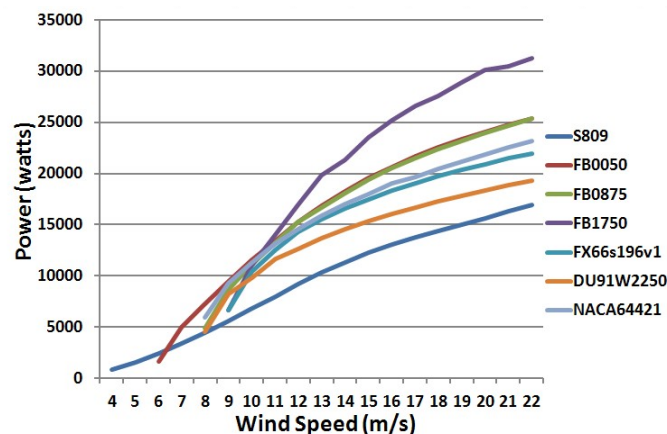Figure 11. Geometric properties of wind turbine using thick airfoil sections

Figure 12. Comparison of power output of a wind turbine of Table 4 with different airfoil sections with the original NREL Phase II wind turbine with S809 airfoil section

The comparison of results in Figure 12 shows that all the wind turbines in Table 4 which employ thick airfoils sections have superior performance than the NREL Phase II wind turbine. Among them, wind turbines with Flat-back airfoils generate greater power than those with other airfoil sections. In particular, the turbine with FB 1750 airfoil section blades generates the largest power output at higher wind speed (greater than 10 m/s). Its power output is almost double compared to that of the original NREL Phase II wind turbine. It can also be noted from Figure 12 that for wind speeds between 8 - 10 m/s, wind turbines in Table 4 with thick airfoil sections generate consistently more power compared to the NREL Phase II turbine with S809 airfoil section for its blades. However at lower wind speeds below 8m/s, there is no appreciable difference in the power generation with change in the blade airfoil section.

Table 5 and Figure 13 show the operating conditions and geometrical properties of the wind turbines with twisted and un-tapered blades using a variety of thick airfoil sections. Figure 14 shows the power output of the wind turbines using different airfoil sections in Table 5 and their comparison with the original NREL Phase III wind turbine with S809 airfoil section for its blades.

Table 5. General characteristics of a wind turbine using thick airfoil sections

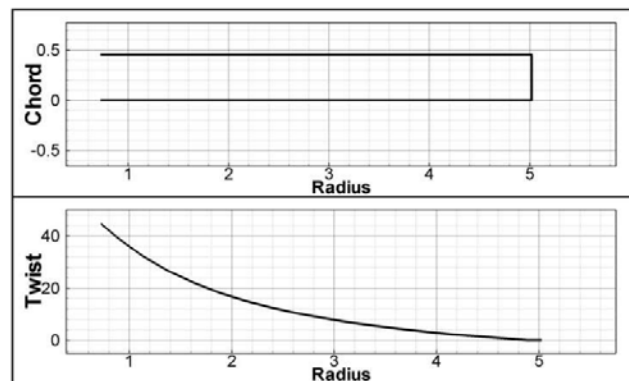|	
Number of Blades	3
Turbine Diameter	10.06m
Rotational Speed	71.3rpm`
Cut-in Wind Speed	6 m/s
Control	Stall Control
Rated Power	19.8kw
Root Extension	0.723m
Blade Set Angle	3 degrees
Twist	44 degrees (max.)
Chord	0.4572@all span location
Airfoil Sections	FB series (FB-3500-0050, FB-3500-0875, FB-3500-1750), FX 66-S196-V1, DU 91-W2-250, NACA 64421

Figure 13. Geometric properties of wind turbine using thick airfoil sections

The comparison of results in Figure 14 shows that all the wind turbines in Table 5 which employ thick airfoils sections have superior performance than the NREL Phase III wind turbine except for the turbines with FB series airfoil blade sections, which only perform better at higher wind speeds (larger than 10m/s). However at wind speed larger than 10m/s, the performance of wind turbines with FB series blade sections is superior. In particular, the turbine with FB 1750 airfoil section blades generates the largest power output at higher wind speed (greater than 10 m/s). Its power output is almost two to three times compared to that of the original NREL Phase III wind turbine. It can also be noted from Figure 14 that for wind speeds between 8 - 10 m/s, wind turbines in Table 5 with thick airfoil sections generate consistently more power compared to the NREL Phase III turbine with S809 airfoil section for its blades. However at lower wind speeds below 8m/s, there is no appreciable difference in the power generation with change in the blade airfoil section.
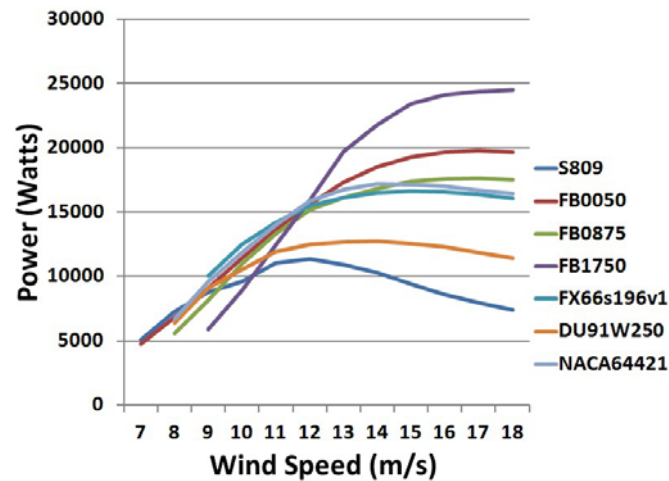
Figure 14. Comparison of power output of a wind turbine of Table 5 with different airfoil sections with the original NREL Phase III wind turbine with S809 airfoil section

Table 6 and Figure 15 show the operating conditions and geometrical properties of the wind turbines with both twisted and tapered blades using a variety of thick airfoil sections. Figure 16 shows the power output of the wind turbines using different airfoil sections in Table 6 and their comparison with the original Risoe wind turbine with NACA 63-2xx series airfoil section for its blades.

The comparison of results in Figure 16 shows that all the wind turbines in Table 6 which employ thick airfoils sections have slightly superior performance than the Risoe wind turbine only at higher wind speeds (larger than 10m/s). However at wind speeds lower than 10m/s, there is no appreciable difference in the performance.

Some parametric studies were also performed to determine the effect of change in turbine diameter and the number of blades on turbine power output. For the study of the effect of change in turbine diameter on power output, the NREL Phase II turbine was selected. Figure 17 shows the variation of power output with wind speed for different turbine diameters. As expected, the wind turbines with larger turbine diameter produce higher power. However it is important to note from Figure 17 that the combined effect of higher wind speed and larger diameter can be very substantial (as well-known from simple analysis); it is validated here by using the more complex BEM code.

For studying the effect of number of blades on the turbine power out, both NREL II and III wind turbines were selected. FB1750 airfoil blade section was chosen because of its outstanding performance in power production. The number of blades was changed from 1 to 5. Figure 18 shows the comparison of the power output of NREL II configuration based wind turbine with different number of blades compared to the original 3-bladed NREL II wind turbine (which uses the S809 airfoil section).

Table 6. Risoe wind turbine general characteristics

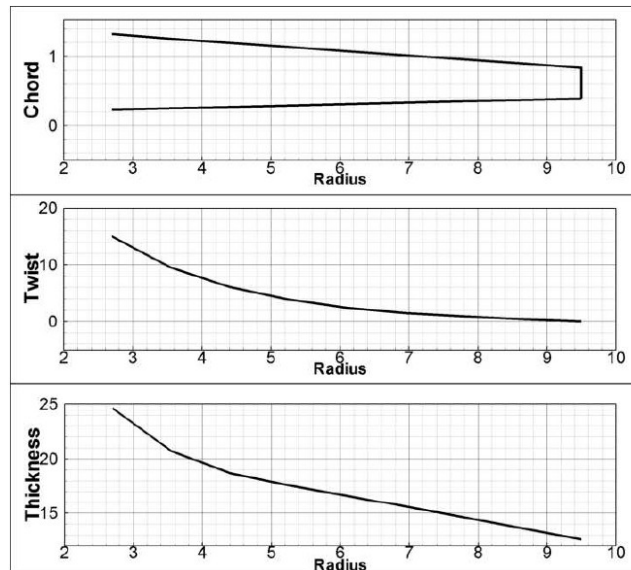|	
Number of Blades	3
Turbine Diameter	19.0 m
Rotational Speed	35.6 and 47.5 rpm`
Cut-in Wind Speed	4 m/s
Control	Stall Control
Rated Power	100 kw
Root Extension	2.3 m
Blade Set Angle	1.8 degrees
Twist	15 degrees (max.)
Root Chord	1.09 m
Tip Chord	0.45 m
Airfoil Sections	FB series (FB-3500-0050, FB-3500-0875, FB-3500-1750), FX 66-S196-V1, DU 91-W2-250, NACA 64421

Figure 15. Geometric properties of wind turbine using thick airfoil sections
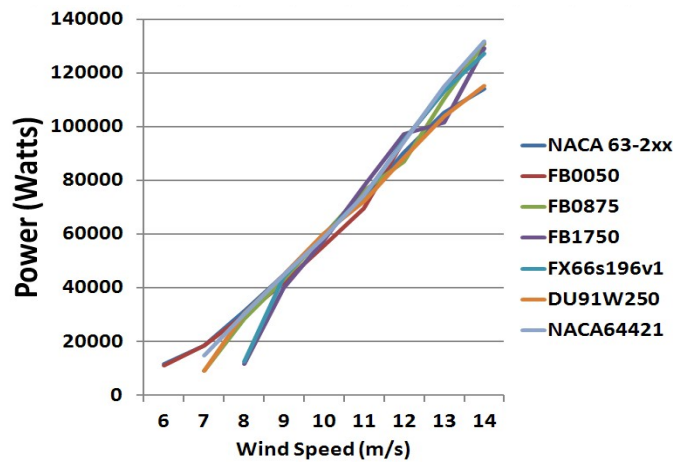

Figure 16. Comparison of power output of a wind turbine of Table 6 with different airfoil sections with the original Risoe wind turbine with NACA 63-2xx airfoil section
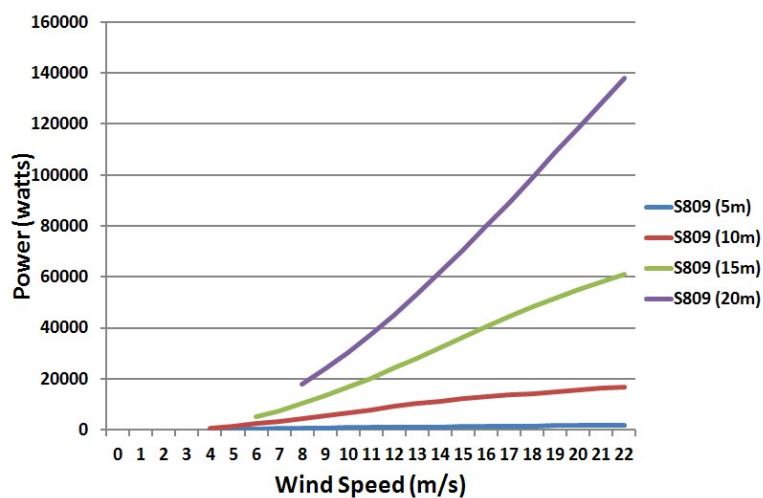

Figure 17. Variation of power output with wind speed for different diameters of NREL Phase II wind turbine
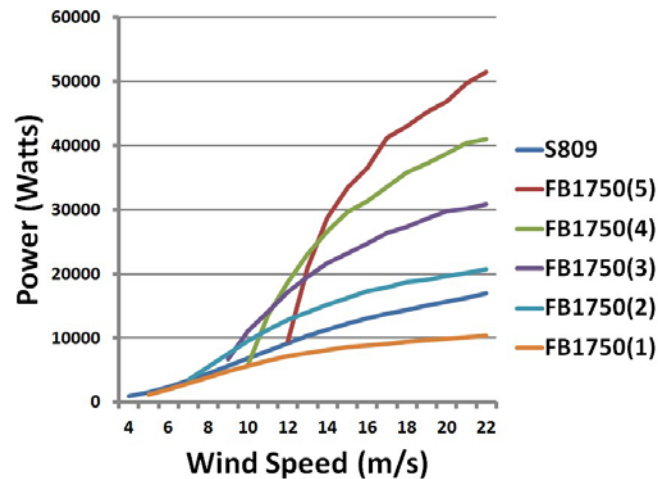
Figure 18. Comparison of power output from original 3-bladed NREL II configuration based wind turbine (with S 809 blade sections) with NREL II wind turbine with 1 to 5 blades (with FB 1750 airfoil section)

Figure 19 shows the comparison of the power output of NREL III - based wind turbine with various numbers of blades with the original 3-bladed NREL III wind turbine (which uses S809 airfoil section). It can be concluded from Figures 18 and 19 that more number of blades tends to increase the power output at high wind speed (greater than 12 m/s) while maintaining or even decreasing the power output at lower wind speeds. Furthermore, as expected, the power output from one-bladed wind turbine is smaller than the original 3-bladed NREL II and III wind turbines even though it employs the FB1750 airfoil as blade cross section. However, one can observe that the two-bladed wind turbines have started to show superior performance at high wind speed. For NREL II configuration based wind turbine, all cases except that of one-blade wind turbine have better power output than the original NREL II turbine for the entire wind speed range, For NREL III configuration based wind turbines, the increase in power output happens only at high wind speeds.
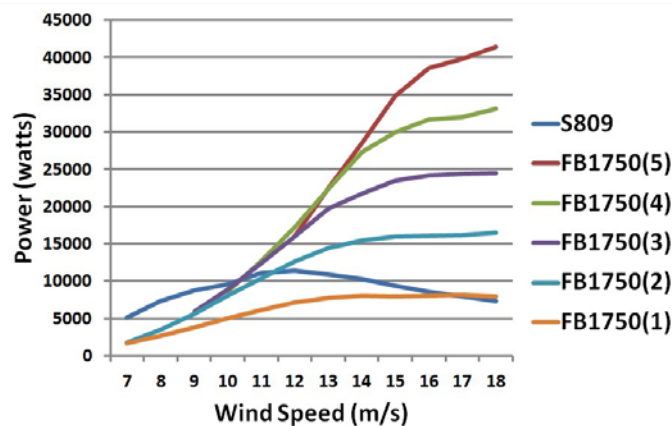

Figure 19. Comparison of power output from original 3-bladed NREL III wind turbine (with S809 airfoil section) with NREL III configuration based wind turbines for different number of blades (with FB1750 airfoil section)

5. Conclusions and future work

The primary focus of this study has been to investigate the effect of blade airfoil sections on power output of a wind turbine. An improved Blade Element Momentum theory based code has been developed for this purpose. The BEM code has been validated by comparing its results with experimental data available for NREL Phase II and Phase III turbines and the Risoe turbine. It is shown that the wind turbines with thick airfoil sections can generate greater power than the original NREL Phase II, Phase III and Risoe wind turbines particularly at higher wind speeds (larger than 10 m/s). In the design of future

more efficient wind turbines, this information can be useful. Some future work may include the evaluation of both twisted and tapered wind turbine blades (used in Risoe wind turbine for example) using other optimized (for C_L/C_D) airfoil sections developed in References [3, 4].

Acknowledgement

References

[1] Energy-XS. Vertical axis wind turbines v/s horizontal axis Wind Turbines. 2010. Accessed from http://www.energyexcess.com/node/7.

[2] Ceyhan O., Sezer-Uzol N., Tuncer I.H. Optimization of horizontal axis wind turbines by using BEM theory and genetic algorithm. Proceedings of the 5th Ankara International Aerospace Conference. METU, Ankara, Turkey, 17-19 August, 2009.

[3] Chen X., Agarwal R. Optimization of flatback airfoils for wind-turbine blades using a genetic algorithm. J. of Aircraft. 2012, Vol. 49, No. 2, pp. 622-629.

[4] Chen X., Agarwal R. Optimization of FX, DU and NACA airfoils for wind turbine blades using a multi-objective genetic algorithm. Proceedings of the 51st AIAA Aerospace Sciences Meeting. Grapevine, TX, 7-10 January 2013. AIAA Paper 2013-0782.

[5] Grasso F. Development of thick airfoils for wind turbines. Proceedings of the 50th AIAA Aerospace Sciences Meeting. Nashville, TN, USA, 9-12, January 2012. AIAA Paper 2012-023.

[6] Baker J.P., Mayda E.A., van Dam, C.P. Experimental analysis of thick blunt trailing edge wind turbine airfoils. ASME J. of Solar Energy Engineering. 2006, Vol. 128, pp. 422-431.

[7] Gooden J.H.M. Experimental low-speed aerodynamic characteristics of the Wortmann FX 66-S-196 VI airfoil. Technical Soaring. 1979, Volume V, No. 3, p. 21.

[8] Timmer W.A., van Rooij R.P.J.O.M. Summary of the Delft University wind turbine dedicated airfoils. ASME J. of Solar Energy Engineering. 2003, Vol.125, pp. 488-496.

[9] Timmer W.A. An overview of NACA 6-digit airfoil series characteristics with reference to airfoils for large wind turbine blades. Proceedings of AIAA 47th Aerospace Sciences Meeting. Orlando, Florida , 5 - 8 January 2009. AIAA Paper 2009-268.

[10] Ingram G. Wind turbine blade analysis using the blade element momentum method. Version 1.1. October 18, 2011.

[11] Moriarty P.J., Hansen A.C. Aerodyne theory manual. Technical Report No. NREL/TP-500-36881. January, 2005.

[12] Schepers J.G. et al. Final report of IEA Annex XVIII: enhanced field rotor aerodynamics database. Technical Report ECN-C-02-016. February 2002. Energy Research Centre of Netherlands.

[13] Bertagnolio F., Sørensen N.N., Johansen J., Fuglsang, P. Wind turbine airfoil catalogue. Tech. Report No. Risø-R-1280(EN), Risø National Laboratory, Roskilde, Denmark, 2001.

[14] Viterna L.A., Janetzke D.C. Theoretical and experimental power from large horizontal axis wind turbines. 1982. NASA TM-82944.
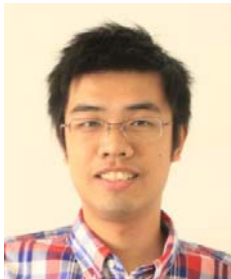
Xiaomin Chen is currently pursuing Ph.D. in the Department of Mechanical Engineering & Materials Science at Washington University in St Louis. He received B.S. in Mechanical Engineering from Shanghai Jiao Tong University, China in 2008 and M.S. in Mechanical Engineering from Washington University in St. Louis in 2010. His research focus is in areas of wind energy and aerodynamics. He is working on shape optimization of wind turbine blades and optimization of wind-farm layouts using CFD and genetic algorithms..
E-mail address: jackmin.chen@gmail.com

Ramesh Agarwal received PhD in aeronautical sciences from Stanford University in 1975. His research interests are in the theory and applications of Computational Fluid Dynamics (CFD) to study the fluid flow problems in aerospace and renewable energy systems. He is currentlythe William Palm Professor of Engineering in department of Mechanical Engineering and Materials Science at Washington University in St. Louis, MO, USA. He is a Fellow of ASME, AIAA, IEEE, andSAE.
E-mail address: rka@wustl.edu